Bulletin of the Seismological Society of America, Vol. 88, No. 6, pp. 1337–1352, December 1998

Earthquake Source Parameters and Fault Kinematics in the Eastern California Shear Zone

by Laura E. Jones and Donald V. Helmberger

Abstract Based on waveform data from a profile of aftershocks following the north–south trace of the 28 June 1992 Landers rupture across the Mojave desert, we construct a new velocity model for the Mojave region that features a thin, slow crust. Using this model, we obtain source parameters, including depth and duration, for each of the aftershocks in the profile and, in addition, any significant ($M > 3.7$) Joshua Tree–Landers aftershock between April 1992 and October 1994 for which coherent TERRAscope data were available. In all, we determine source parameters and stress drops for 45 significant ($M_w > 4$) earthquakes associated with the Joshua Tree and Landers sequences, using a waveform grid-search algorithm. Stress drops for these earthquakes appear to vary systematically with location, with respect to previous seismic activity, proximity to previous rupture (i.e., with respect to the Landers rupture), and with tectonic province. In general, for areas north of the Pinto Mountain fault, stress drops of aftershocks located off the faults involved with the Landers rupture are higher than those located on the fault, with the exception of aftershocks on the newly recognized Kickapoo (Landers) fault. Stress drops are moderate south of the Pinto Mountain fault, where there is a history of seismic swarms but no single throughgoing fault. In contrast to aftershocks in the eastern Transverse ranges, and related to the 1992 Big Bear, California, sequence, Landers events show no clear relationship between stress drop and depth. Instead, higher stress-drop aftershocks appear to correlate with activity on nascent faults or those that experienced relatively small slip during mainshock rupture.

Introduction

Stress drop and style, depth, and timing of aftershock activity relative to mainshock rupture plane or fault trace yield clues about how the regional "stress budget" is settled following a large earthquake. Aftershock stress drops vary with source area and tectonic environment (Lindley and Archuleta, 1992), reflecting regional differences in the source properties of small earthquakes.

The M_w 7.3 Landers earthquake of 11:58 GMT, 28 June 1992, was preceded by the 23 April 1992 Joshua Tree mainshock (M_w 6.1) that is now considered a precursory event (Stein *et al.,* 1992) with its own substantial fore- and aftershock sequence. The Landers event was followed by tens of thousands of aftershocks (Kanamori *et al.,* 1992; Hauksson *et al.,* 1993; Sieh *et al.,* 1993), many in areas with no surface rupture (e.g., Big Bear region, see Fig. 1). Stress drops and source parameters of Joshua Tree–Landers aftershocks provide information critical to understanding fault kinematics in the Eastern California Shear Zone (ECSZ), which encompasses the Landers rupture area and may extend beneath the eastern Transverse ranges (Jones and Hough, 1995).

Because data for the present study come from a sparse array (three to five TERRAscope stations), care must be taken when modeling available data to ensure accuracy in depth and source mechanism estimation. A standard one-dimensional model such as the Southern California Model may often be used to satisfactorily approximate broadband waveforms at near-regional distances (see Dreger and Helmberger, 1991). However, waveform misfit introduced by use of an inappropriately thick crust, for example, more adversely affects quality and robustness (error) of source solutions obtained from small datasets. A regional model is thus necessary for this work.

In this article, we present source parameters, including duration, depth, and stress drop, obtained for Landers and Joshua Tree events using a new Earth model designed to fit near-regional data with source–receiver paths in the Mojave. The article treats events from this large sequence as follows: moving chronologically from the April 1992 Joshua Tree preshock to Landers aftershocks, first south and then north of the Pinto Mountain Fault, including a cluster of events in the Barstow region and triggered earthquakes on the Garlock fault. Events occurring within the ECSZ are compared with

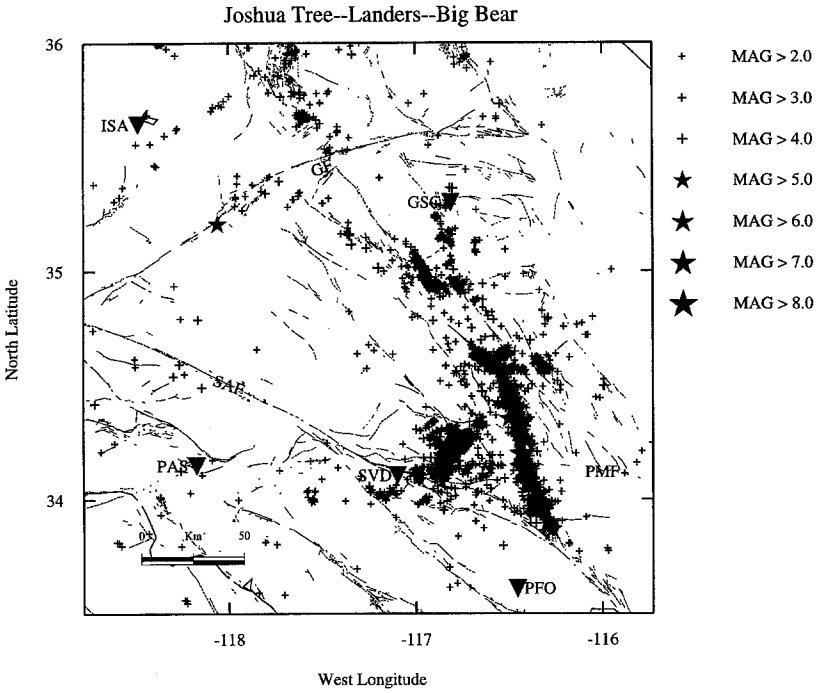

Figure 1. Location map showing main events and aftershocks from the Joshua Tree, Landers, and Big Bear sequences. Map covers seismicity from 23 April 1992 to 31 December 1992. Faults are indicated as follows: SAF (San Andreas fault), GF (Garlock fault), and PMF (Pinto Mountain fault).

Landers aftershocks occurring in the Eastern Transverse Ranges and comprising the 1992 Big Bear, California, sequence. Finally, we correlate aftershock stress drop with timing and proximity to mainshock rupture.

Data and Observations

Larger fore- and aftershocks from the Joshua Tree and Landers sequences were recorded on scale by six broadband TERRAscope stations (GSC, ISA, PAS, PFO, SVD, and SBC). In this study, we use records from the first five stations (Fig. 2), because records from station SBC are low signal to noise and contaminated by propagation through basin structure. For TERRAscope stations Goldstone (GSC) and Pinyon Flats (PFO), due north and nearly south of the Landers rupture, we construct profiles of aftershocks from the Landers earthquake. These include earthquakes in areas associated with Landers surface rupture (north of the Pinto Mountain fault), south of the Pinto Mountain fault, and associated with the Barstow swarm. These earthquakes form rough profiles following the general trend of the Landers rupture.

Before modeling, the records were processed as follows: instrument gain was removed from the raw velocity records; they were detrended and integrated once. A butterworth bandpass filter with corners at 0.04 and 7 Hz was applied twice. Filtering was minimal so that the broadband nature of the records might be preserved. In cases where the event was fairly large and close to a particular station, low-gain records (accelerograms) from TERRAscope were used. They were processed similarly: gain removed, detrended, twice integrated, and bandpass filtered.

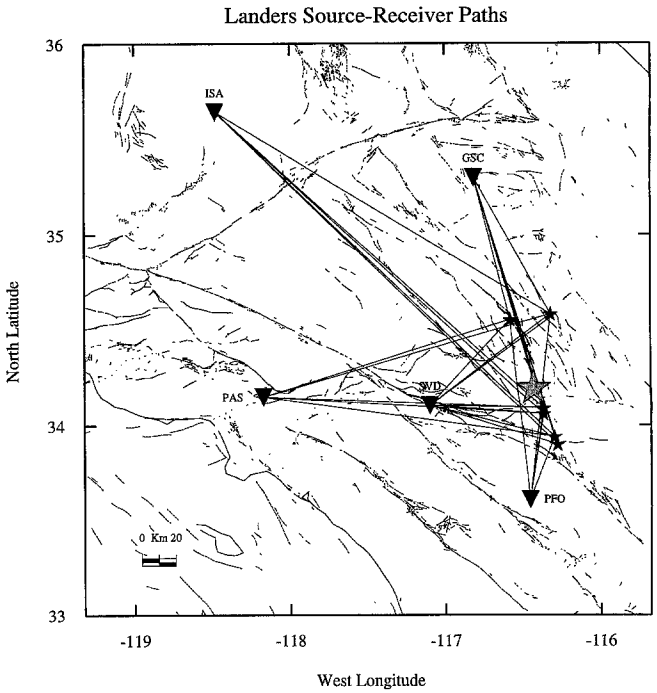

Figure 2. Source–receiver paths for the profiles used in source modeling and in the construction and testing of the Mojave model. Stations GSC, PFO, and SVD were used primarily in the estimation of source mechanisms for Landers and Joshua Tree events. Stations ISA and PAS were included as needed, to create a robust solution in cases where the solution appeared unstable. Source-event paths for stations GSC and PFO were used in the development of the Mojave model (Table 1).

Analysis

The Mojave Model

Studies to date on moderately sized southern California earthquakes suggest that a relatively simple, plane-layered velocity model often explains the observed waveforms satisfactorily. For example, waveforms from the 28 June 1991 Sierra Madre earthquake, centered within the TERRAscope array, were well modeled at several stations by the standard southern California model (Hadley and Kanamori, 1977; Dreger and Helmberger, 1991). Studies of several other events also suggest that this standard model is appropriate for use in the southern California region (Jones and Helmberger, 1992; Song and Helmberger, 1997). However, this standard model did not work well for Landers aftershocks recorded at stations in the Mojave Desert.

High-quality aftershock data recorded at local to regional distances gave us the opportunity to develop a path-specific model for the Mojave region. Aftershocks from the Landers sequence recorded at TERRAScope stations GSC and PFO were assembled, and profiles of broadband data were constructed from events located and recorded in the Mojave block, as such possessing source–receiver paths contained entirely within this region (Fig. 2). Records at these distances (35 to 165 km, see Fig. 3) are dominated by crustal arrivals and Moho-reflected arrivals, which suggest a crust thinner (depth to the Moho is 28 km) and slower than the standard southern California model (Hadley and Kanamori, 1977; Dreger and Helmberger, 1991) and lacking the gradient at the base of the crust (Conrad) that characterizes the widely used standard model.

The choice of stations GSC and PFO for this modeling task was natural and fortunate, because Landers events recorded at these two stations form north–south profiles. The locations of stations GSC and PFO due north and south (respectively) of the aftershocks, however, practically insures that many events will be *P*-wave nodal at both stations, because many have northerly strikes (parallel to the Landers rupture). Conversely, the tangential component is near maximum, so it is easily modeled (Fig. 3).

In order to construct the model, we first make an estimate of the source mechanisms for the profile events, assuming the standard southern California model (Table 1). We subsequently refine the original source and moment estimations for the profile events using the new model; these estimations show improved waveform fit and lower error.

The Mojave model (Table 2) has a thinner crust (28 km versus 35 km) than the standard California model and slower *P*- and *S*-wave crustal velocities. It also lacks the gradient at the base of the crust (the so-called Conrad discontinuity) that characterizes the standard model.

Determination of Source Parameters

Average source parameters and depths for the small and moderately sized earthquakes studied here are estimated using a direct grid-search method (Zhao and Helmberger,

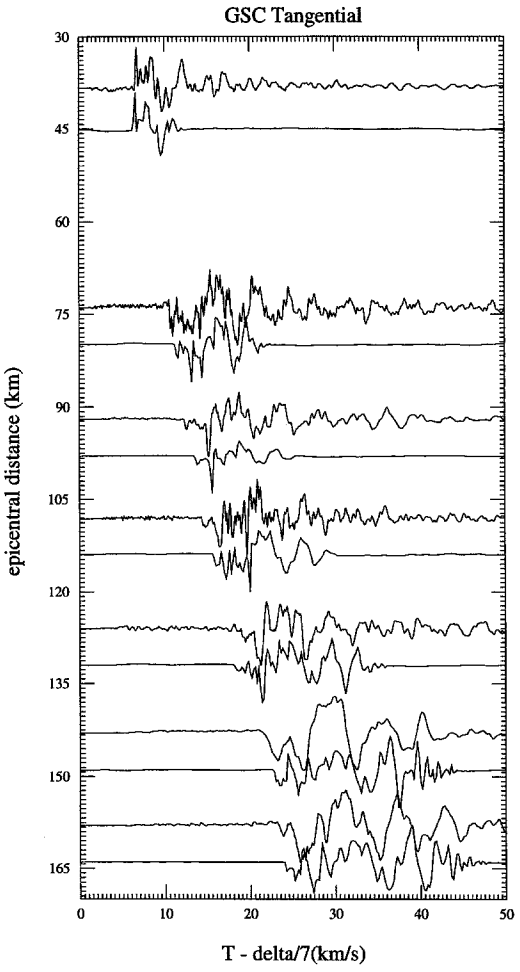

Figure 3. Profile of Landers data and modeling for the tangential component of displacement recorded at station GSC. This profile ranges north to south, with source–receiver distances ranging from 40 to 160 km and source depths between 8 and 11 km, roughly average for this sequence. Source mechanisms used in the modeling are computed using the methods discussed in text. Records are modeled and shown broadband; observed displacement records are shown in bold line above synthetics. Synthetics are generated using the Mojave model (this article, Table 1) and the frequency-wavenumber method.

Table 1
Standard Southern California Model

V_p (km/sec)	V_s (km/sec)	ρ (g/cm^3)	Depth (km)
5.50	3.18	2.40	5.5
6.30	3.64	2.67	16.0
6.70	3.87	2.80	32.0
7.85	4.50	3.42	half-space

Table 2
Mojave Model

V_p (km/sec)	V_s (km/sec)	ρ (g/cm^3)	Depth (km)
5.00	2.60	2.40	2.5
5.50	3.45	2.40	5.5
6.30	3.60	2.67	28.0
7.85	4.40	3.42	half-space

1994). This algorithm selects source parameters that minimize the L1 and L2 norms between observations and synthetic waveforms, using three-component P_{nl} and whole waveforms to produce a stable solution from a relatively sparse dataset and an imperfect structural model (Jones *et al.*, 1993; Jones and Helmberger, 1992; Zhu and Helmberger, 1995; Song and Helmerger, 1997). Note that P_{nl} is defined as the first part of the regional waveform, from where the record is dominated by P phases (P_n) to where the motion contains progressively more SV contributions (PL) (Helmberger and Engen, 1980). The procedure desensitizes the misfit in timing between principal crustal arrivals in the data and synthetic by fitting portions of the waveforms independently. Source durations for the grid search are initially estimated from the width of the direct pulse. Refined durations (see later) are then iteratively fed back into the grid-search scheme to recompute source parameters. Given the development of Green's functions specific to paths within the Mojave block, we use a sparse array (three to five stations) and the data both broadband and after convolution with a long-period Press-Ewing ("LP3090": 30-sec period, 90-sec galvenometer) instrument response. The long-period energy is modeled because these solutions are often more stable than the broadband solutions, as detailed below, though we seek consistency between broadband and long-period solutions. Broadband solutions were occasionally used for the smallest events, in cases where energy was lacking in the long-period bandpass, and the broadband solution showed greater consistency between stations.

Estimation of Source Depths

We determine source depths directly from the surface-reflected phases S_mS or sS_mS and by cycling through depth-dependent Green's functions (2, 5, 8, 11, 14, and 17 km) during the grid-search procedure itself. To speed the process, we employ a catalog of Green's functions appropriate to the Mojave model, which are computed at 5-km distance intervals from 35 to 400 km and assuming source depths listed earlier. In general, the mechanisms and depths obtained in this study are consistent with those obtained by other workers. In some cases, however, the depths we obtain are not as shallow as those obtained by others (Thio, 1996, by surface-wave inversion; Hauksson, 1993, via inversion of short-period network data). As an example, we show modeling for the 5 August 1992, 22:22 GMT Landers aftershock (Fig. 4). Fits for all three components (including the radial) are shown. Error space for the depth determination (Fig. 5) shows a clear minimum at between 5 and 8 km for this event, though others place the depth of this event at less than 5 km (Hauksson, 1994). P_{nl} to surface-wave amplitude ratios on the vertical and radial components of motion suggest a depth of about 5 km, while ratios of body-wave to Love-wave amplitudes suggest a depth of 8 km or greater. Indeed, separation between S_mS and sS_mS phases on the tangential components at stations PFO (epicentral distance 155 km), ISA (160 km), and PAS suggest a depth arguably deeper than 8 km.

Within the error imposed by the depth gridding on our solution space (every 2 to 3 km), we believe that our depths, obtained from a grid-search routine that is tantamount to direct waveform modeling, are reliable. There is substantial difference in the separation between S_mS and sS_mS phases for events at source depths of, say, 2 and 5 km. Our estimates suggest that all of the $M > 3.7$ events we studied had depths of 5 km or greater, and average depth is about 8 km.

Source Duration and Relative Stress Drop

Source durations are obtained by methods ranging from direct measurement of source pulse (e.g., Smith and Priestly, 1993; Hardebeck and Haukssen, 1997) to determination of corner frequency (e.g., Hough and Dreger, 1995). In this study, average source durations are determined from a simple comparison of energies (see also Jones and Helmberger, 1996; Zhao and Helmberger, 1996; Song and Helmberger, 1997). In this procedure, we equalize energy content across different frequency bands between data and synthetics. First, a short-period Wood–Anderson instrument response (WASP) and a long-period instrument response (LP3090) are applied to data and synthetics to compute short- and long-period energy, respectively. The P_{nl} waves (in velocity) from each station are then compared with synthetic P_{nl} waveforms (velocity):

$$\text{Ratio} = \frac{E_{(\text{obs})}}{E_{(\text{syn})}}, \tag{1}$$

where

$$E = \frac{\int_{t_{pn}}^{t_{PL}} [V_{(sp)}]^2 dt}{\int_{t_{pn}}^{t_{PL}} [V_{(lp)}]^2 dt}. \tag{2}$$

$V_{(sp)}$ is the observed (or synthetic) P_{nl} wave, in velocity, convolved with a short-period Wood–Anderson response, and $V_{(lp)}$ is the observed (or synthetic) P_{nl} wave, in velocity, convolved with an LP3090 instrument response. The time function for the synthetic waveform is adjusted until the ratio of energies is unity (symmetric trapezoidal time functions are assumed). An average for the radial and vertical com-

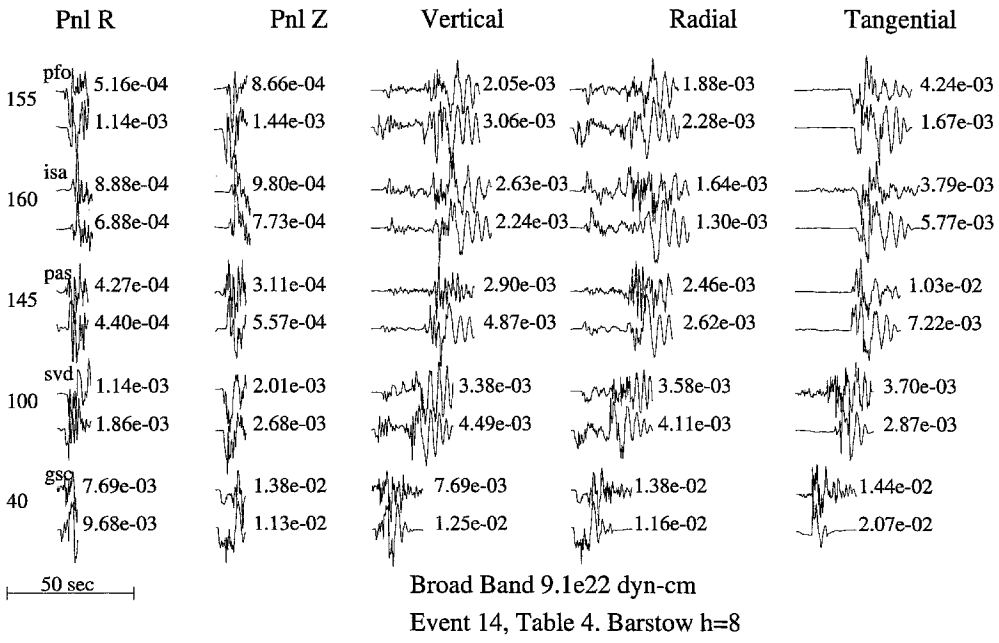

Figure 4. Broadband modeling for the 5 August 1992 22:22 (Barstow) aftershock. Source depth was estimated at between 5 and 8 km by cycling through synthetics appropriate to source depths from 2 to 17 km and finding a minimum error solution. Event duration was estimated first by measuring the direct pulse, then by the energy method described in this article. Synthetics are generated using the F-K method and the Mojave model. This plot shows waveform fits assuming a depth of 8 km.

ponents is found at each station, and the resulting values for each reporting station are then averaged.

The procedure yields a conservative estimate of source-time duration and thus stress drop and is limited to source triangles no shorter than 0.20 sec in duration. This limitation is imposed by the computational technique used and, to a lesser extent, by the frequency content available in the synthetic Green's functions. Other researchers using this method found good correlation between source durations determined via comparison of energies and those determined by measuring the width of the direct pulse at local stations (Song and Helmberger, 1997), except for a (constant) offset. The offset may be explained by the fact that the synthetics used in the energy method do not contain scattering (Song and Helmberger, 1997). Note that source durations obtained by energy comparison are systematically smaller than those obtained via direct measurement. The energy method thus provides a reliable estimate of relative source duration between events.

Assuming minimal attenuation, the width of the observed P or S pulse is proportional to the source dimension and thus source duration. The actual pulse width, as observed, may depend on factors as diverse as crustal attenuation, rupture mode, length and velocity, and source complexity. On average, however, one may assume a linear relationship between pulse width and source dimension. Indeed, Cohn *et al.* (1982), assuming a circular fault (Brune, 1970), obtained the relation

$$\tau = \frac{2.62a}{\beta}, \tag{3}$$

where τ is the source duration in seconds, a is the radius in kilometers, and β is the shear velocity local to the source region. Solving for a in terms of τ, assuming a shear velocity of 3.5 km/sec and substituting the result into the expression for stress drop on a circular fault (Eshelby, 1957),

$$\Delta\sigma = \frac{7M_o}{16a^3}, \tag{4}$$

we obtain (in bars, given 1 bar $= 10^6$ dyne-cm^2)

$$\Delta\sigma = \frac{1.84 \times 10^{-22}M_o}{\tau^3}. \tag{5}$$

An estimate of the error inherent in the computation of relative stress drop is found as follows. Assuming that the error in M_0 and τ are to first-order independent, we can write the error as the vector sum of error in $\Delta\sigma$ due to error in the estimates of M_0 and τ, respectively:

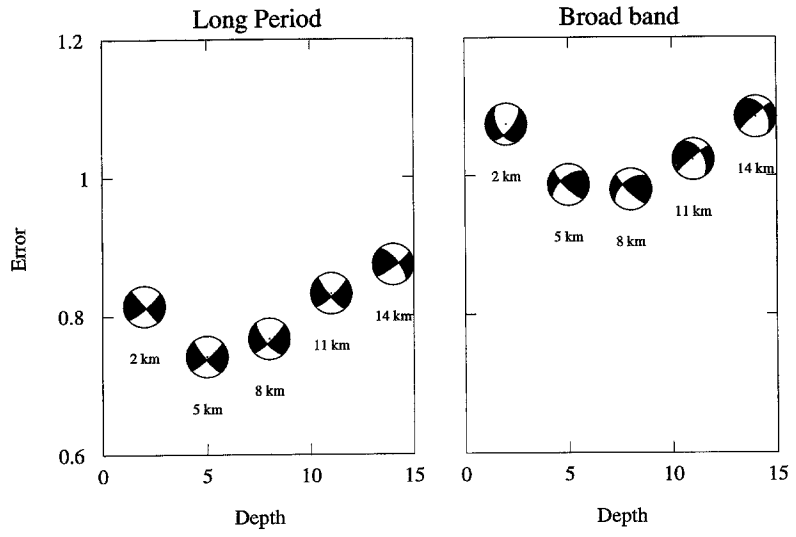

Figure 5. Error space for the 5 August 1992, 22:22 (Barstow) event. Source depths are indicated across the bottom of the plot and error on the vertical axis. The left-hand panel shows error from the long-period solution, and the right-hand panel shows error from the broadband solution. Focal spheres appropriate to each depth indicate data points; note that long-period focal spheres show more consistency.

$$\delta[\Delta\sigma] = \sqrt{\left(\frac{\delta[\Delta\sigma]}{\delta\tau}\Delta\tau\right)^2 + \left(\frac{\delta[\Delta\sigma]}{\delta M_o}\Delta M_o\right)^2}. \quad (6)$$

Taking partial derivatives of (5) with respect to τ (holding M_0 constant) and M_0 (holding τ constant), substituting into (6) and simplifying,

$$\delta[\Delta\sigma] = \sqrt{\left[\frac{3\Delta\sigma}{\tau}\Delta\tau\right]^2 + \left[\frac{\Delta\sigma}{M_o}\Delta M_o\right]^2}. \quad (7)$$

Factoring out a $\Delta\sigma$ in (7), we obtain percentage error:

$$\frac{\delta[\Delta\sigma]}{\Delta\sigma} = \sqrt{\left[\frac{3}{\tau}\Delta\tau\right]^2 + \left[\frac{1}{M_o}\Delta M_o\right]^2}. \quad (8)$$

Small events with shorter time functions had relatively greater error associated with the determination of source duration and often greater error associated with the determination of moment (due to poor signal to noise). For the Joshua Tree sequence, for example, we obtain errors ranging from 67%, for an event with 58% error in the moment estimation and M_b 4.3, to 32%, for an event with 29% error in moment estimation and M_b 4.5. Larger events are predictably associated with smaller error. The 11 July 1992, M_b 5.1 Garlock fault event had an uncertainty in moment estimation of 24% and an error in stress-drop estimation of about 20%.

We use relative stress drop along with source parameters in the following discussion to explore the relation between source type, depth, location, and relative energy release in the eastern California shear zone.

Results and Discussion

Coulomb stress changes caused by four $M > 5$ earthquakes preceding the Landers mainshock (i.e., the 1975 M_L 5.2 Galway Lake, 1979 M_L 5.2 Homestead Valley, M_L 6 North Palm Springs, and M_L 6.1 Joshua Tree earthquakes) progressively increased stresses at the site of the future Landers epicenter (King *et al.*, 1994). In turn, changes in static stresses caused by the Landers event triggered the Big Bear event within hours of the Landers mainshock, and earthquakes as far away as the western Garlock fault and Yucca Mountain in the ensuing months (Hill *et al.*, 1993; Gomberg and Bodin, 1994).

As discussed later, Joshua Tree sequence seismicity moved northward in the months following the Joshua tree mainshock, culminating in clusters of aftershocks just north of the Pinto Mountain fault and within the Landers epicentral area in early June of 1992. Hours before the Landers mainshock, a cluster formed at what later became the Landers epicenter (Hauksson *et al.*, 1993). The Landers earthquake involved rupture on five separate faults north of the Pinto Mountain fault, with a small amount of displacement south of the Pinto Mountain fault on the Eureka Peak fault (Fig. 6). The latter rupture may not have occurred entirely during the mainshock but may have been associated with an M 5.7 aftershock occurring minutes after the mainshock (Hough *et al.*, 1993).

We divide our discussion of the Landers sequence into four portions: aftershocks south of the Pinto Mountain fault, including the Joshua Tree preshock sequence, and associated with minimal displacement; aftershocks north of the Pinto Mountain fault, associated with the Landers rupture, aftershocks north and east of the mapped Landers rupture, in the Barstow and Calico-Pisgah fault clusters, respectively; and aftershocks or triggered events along the Garlock fault.

Joshua Tree Sequence

The Joshua Tree sequence began on 23 April 1992 at 02:25 GMT with an M_w = 4.3 foreshock. This event occurred at a location just south of the Pinto Mountain fault

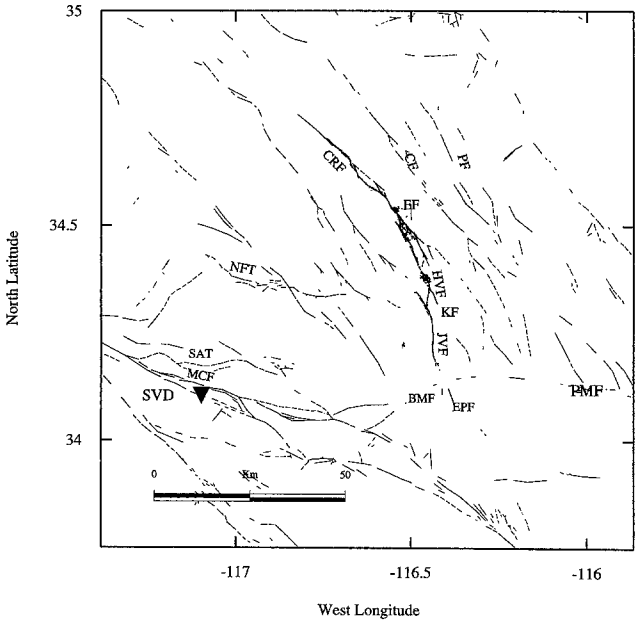

Figure 6. Location map showing faults active during the Joshua Tree, Landers, and Big Bear sequences. Faults are indicated as follows, clockwise from lower left: MCF, Mill Creek fault; SAT, Santa Ana Thrust; NFT, North Frontal Thrust; CRF, Camp Rock fault; CF, Calico Fault; PF, Pisgah fault; EF, Emerson fault; HVF, Homestead valley fault; KF, Kickapoo (Landers) fault; JVF, Johnson Valley fault; PMF, Pinto Mountain fault; EPF, Eureka Peak fault; and BMF, Burnt Mountain fault. The Garlock fault is shown in Figure 1.

(−116.32° W, 33.94° N) and north of the Coachella Valley segment of the San Andreas fault, within the Little San Bernardino Mountains, in a region that has historically seen frequent earthquake swarms. It was followed by a number of additional smaller foreshocks, then within 2.5 h by the nearly colocated M_w = 6.1 Joshua Tree mainshock (Mori, 1994). The Joshua Tree mainshock had no observed surface rupture, though a 10- to 12-km south-to-north subsurface fault plane, striking roughly N20°W, was inferred from the distribution of early aftershocks (Wald, personal comm., 1992; Hauksson *et al.,* 1993; Hough and Dreger, 1995).

The mainshock was followed by a sustained and powerful aftershock series that comprised at least 28 aftershocks of $M > 3.7$, 10 of which were M 4.0 to M 4.7. Joshua Tree aftershocks partially overlap those from the later Landers earthquake, with a cluster of aftershocks, including one event above M 4, developing north of the Pinto Mountain fault and slightly east of the Landers mainshock location in early June (e.g., Fig. 7a, aftershock number 9). $M > 3.9$ aftershocks form two separate clusters south of the Pinto Mountain fault that are filled in by later aftershocks from the Landers earthquake (Fig. 7b). The Joshua Tree series is dominated by moderate to deep (source depth 8 to 14 km) strike-slip and oblique-slip events. Stress drops for these earth-

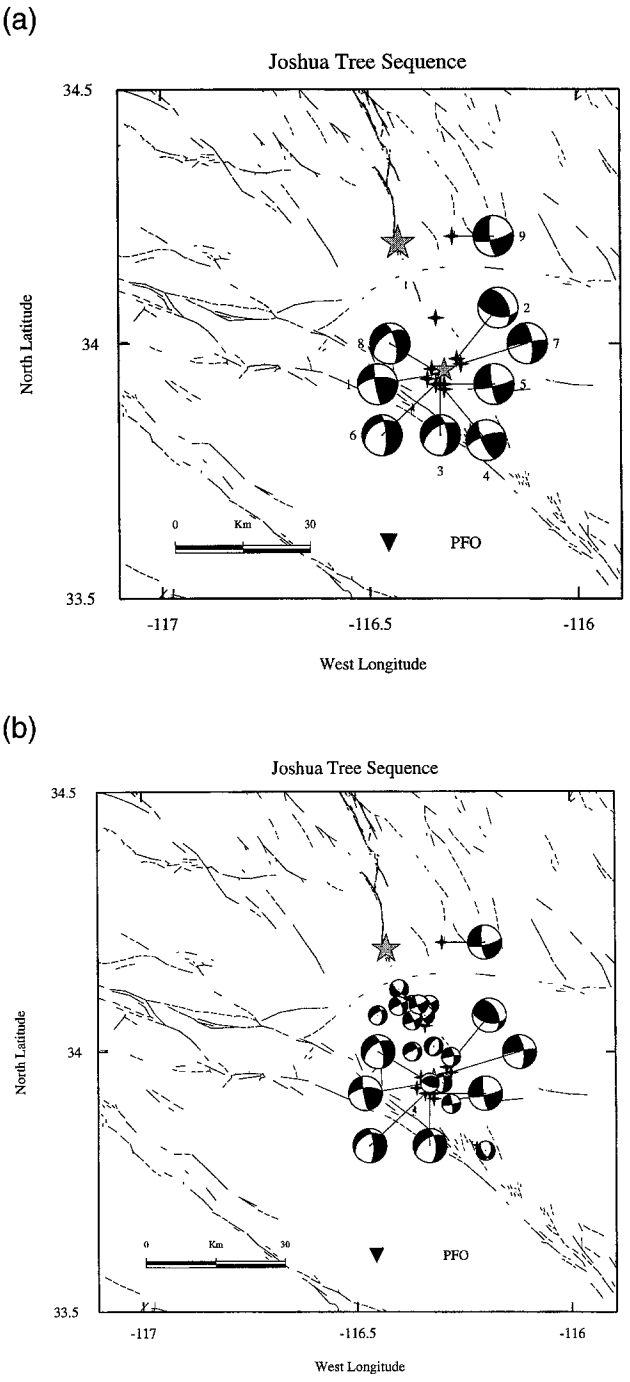

Figure 7. (a) Location map showing Joshua Tree aftershocks. Aftershocks are numbered in order of occurrence and are listed in this order in Table 3. Large filled star is location of Landers mainshock; small filled star is location of Joshua tree preshock. (b) Relative locations of Landers and Joshua Tree aftershocks. Joshua Tree aftershocks are indicated with larger spheres; epicentral locations are crosses. Landers aftershocks in this area are smaller focal spheres. Size of focal sphere is not related to event magnitude.

quakes are on the order of 10 to 100 bars, with an average of 30 bars.

Events of the Joshua Tree sequence are now viewed as preshocks to the later Landers mainshock. While the Landers mainshock apparently either recharged or reactivated aftershock activity in the Joshua Tree region (Hauksson, 1994), $M > 3.8$ aftershocks from the Joshua Tree and later Landers events can be viewed as distinct populations. Spatially, they occupy distinct but adjoining volumes rather than overlapping completely (Figs. 7b and 8). Their mechanisms are similar, presumably strike slip on north to northwest-striking planes, though Joshua Tree aftershocks are on average deeper (Tables 3 and 4). The presence of several $M > 4$ Landers aftershocks in the Joshua Tree epicentral region supports post-Landers reactivation of stresses immediately local to the Joshua Tree epicentral area. These $M > 4$ events are not numerous; however, they are low in stress drop relative to other aftershocks south of the Pinto Mountain fault and are generally not vertical strike slip.

Landers Events South of the Pinto Mountain Fault

Following the Landers mainshock, large ($M > 4.5$) aftershocks were more common south of the Pinto mountain fault than north (Figs. 8, 9, and 12). Almost 76% of the total aftershock energy released post-Landers was released south of the mainshock epicenter, with about 40% of the energy release distributed between the Pinto Mountain fault and the Joshua Tree epicenter (Ma, 1993).

A tight and dense cluster of early aftershocks formed near the epicentral locations of the events on the Eureka Peak and Burnt Mountain faults, as observed in the immediate aftermath and epicentral location of the (northern) Landers mainshock (Fig. 8). Unlike the Landers epicentral area, however, large ($M \geqq 4$) aftershocks continued in this southern region for many months.

Aftershocks extend roughly 40 km south of the mainshock epicenter, forming a NW–SE-trending swath 5 to 15 km in width (Hauksson *et al.*, 1993). We present source parameters, depths, durations, and relative stress drops for 14 $M_w \geqq 3.7$ aftershocks occurring south of the Pinto Mountain fault, including an M_w 4.5 event on 21 August 1993 (Fig. 9, Table 4, event number 13) and two events in August 1994 (Fig. 9, Table 4, events 14 and 15). Events studied suggest a fairly heterogeneous sequence, though oblique strike-slip events are most numerous. These oblique events are consistent in strike direction; all strike NW, presumably in the same direction as the Joshua Tree mainshock (N20°W) and with strike-slip events associated with the Joshua Tree sequence (Figs. 7a and 7b).

Like those estimated for Joshua Tree aftershocks, relative stress drops for Landers aftershocks south of the Pinto Mountain fault are on the order of 10 to 100 bars, with an average of about 67 bars for aftershocks within the first year of the mainshock and an average of 60 bars for aftershocks through 1994. Lowest stress-drop events are associated with either the epicentral region of the southern rupture (Fig. 7b)

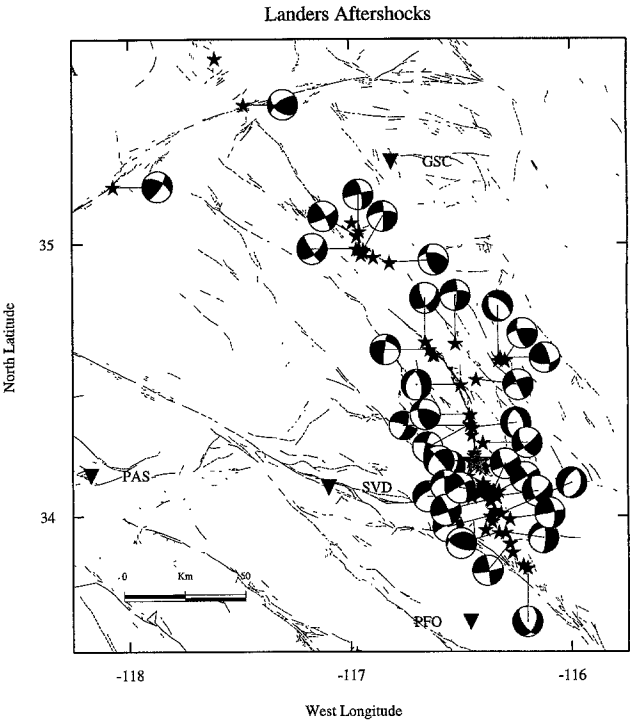

Figure 8. Map of locations and focal spheres for the 34 Landers-related Mojave events discussed here, including two earthquakes on the Garlock fault. Epicentral locations are shown as filled (black) stars. The Landers mainshock is shown as a filled (gray) star. The sequence shown here includes events occurring from June 1992 through October 1994. These events will be further broken down and discussed by location and order of occurrence (i.e., Figs. 11 and 13).

or the area active during earlier Joshua Tree sequence (including the Joshua Tree mainshock) located south of the southern rupture. High stress-drop earthquakes (events 2, 9, and 10) lie west and nearly on the periphery of the low stress-drop cluster associated with the Eureka Peak rupture (i.e., events 3, 4, 5, 8, and 12) as seen in Figure 9. Event 14 (on the periphery of former Joshua Tree seismicity) is unusually low stress drop but occurred after much of the sequence had exhausted itself: this late M_w 3.7 event occurred in August 1994, at a depth of 8 km. On average, Landers events are higher stress drop than Joshua Tree events (Tables 3 and 4, Fig. 10), again supporting the notion that the Landers mainshock may have recharged this historically active region.

In map view, southern Landers events do not define any one fault plane; rather they rerupture areas associated with the Joshua Tree sequence and fill in unaffected regions north toward the Pinto Mountain fault. The history of seismic activity in the region, the present heterogeneity of faulting, and the lack of any one well-defined fault plane suggest that displacement south of the Pinto mountain fault may be accommodated gradually (i.e., in small increments) across a number of small subsurface faults. The gap in large after-

Table 3
Joshua Tree Aftershocks, $M_w > 4$

No.	Date	M_w	τ, $\Delta\sigma$ (s, bars)	θ	δ	λ	Location Depth (km)	Location Latitude (°N)	Location Longitude (°W)
1.	92042302	4.3	0.45, 74	170	82	154	12	33.94	116.33
2.	92042318	4.0	0.45, 19	334	50	130	8	33.97	116.29
3.	92042606	4.5	1.15, 10	354	60	224	8	33.92	116.33
4.	92042703	4.3	1.10, 4	156	74	162	5	33.91	116.34
5.	92050416	4.8	0.80, 70	170	80	190	14	33.92	116.32
6.	92050602	4.5	0.90, 21	356	72	238	11	33.92	116.32
7.	92051202	4.3	0.80, 13	352	70	184	8	33.96	116.28
8.	92051815	4.7	0.80, 55	346	66	224	11	33.95	116.35
9.	92061100	4.4	1.10, 6	172	74	196	9	34.21	116.30

Table 4
Landers Events, South of Pinto Mountain Fault

No.	Date	M_w	τ, $\Delta\sigma$ (s, bars)	θ	δ	λ	Location Depth (km)	Location Latitude (°N)	Location Longitude (°W)
1.	92063011	4.2	0.35, 85	353	51	215	14	34.07	116.45
2.	92063014	5.1	1.0, 90	350	45	200	7	34.00	116.37
3.	92070612	4.2	0.60, 28	330	76	182	8	34.09	116.33
4.	92070619	4.3	0.60, 28	160	62	208	9	34.07	116.34
5.	92071002	3.9	0.50, 10	132	70	218	11	34.12	116.40
6.	92072418	4.9	1.0, 52	351	80	173	8	33.90	116.28
7.	92072504	4.7	1.0, 25	2	76	238	8	33.94	116.30
8.	92072818	4.7	1.0, 25	310	40	100	5	34.09	116.37
9.	92081106	4.1	0.40, 45	336	80	170	8	34.06	116.37
10.	92081508	4.5	0.35, 346	338	58	190	6	34.088	116.403
11.	92090912	4.2	0.50, 38	112	62	110	8	33.94	116.33
12.	92091508	5.2	1.50, 30	156	76	188	8	34.09	116.35
13.	93082101	4.5	0.65, 60	208	54	278	9	34.010	116.32
14.	94080715	3.7	0.60, 4	352	64	184	8	33.99	116.28
15.	94081508	3.8	0.25, 76	146	64	240	9	33.81	116.20

shocks across the Pinto Mountain fault (Fig. 9) suggests that Landers rupture may not continue across the fault and that displacement south of the Pinto Mountain fault may be primarily associated with aftershock activity.

Landers Events Occurring North of the Pinto Mountain Fault

Rupture along the five faults active in the Landers mainshock [from south to north, the Johnson Valley fault, the Kickapoo (Landers) fault, the Homestead Valley fault, the Emerson fault, and the Camp Rock fault] extended roughly 60 km NNW across the Mojave desert north of the Pinto Mountain fault (Figs. 6 and 11). Large ($M > 3.9$) aftershocks along the trend of the Landers rupture are common in three general areas: close to the mainshock epicenter (early aftershocks, within the first 24 to 48 h); at fault ends, including the termination of the Johnson Valley fault and the very active Kickapoo (Landers) fault; and the northern extent of rupture, at the northern terminus of the Camp Rock fault (Figs. 6 and 12). Landers aftershocks north of the Pinto Mountain fault (discounting events on the Garlock) are higher stress drop than southern Landers aftershocks, with on average of 95 bars for events occurring in the first year after the mainshock (Fig. 10, Table 5).

Mainshock Epicentral Area (Johnson Valley Fault). According to Wald and Heaton (1994), the Landers mainshock initiated on the Johnson Valley fault (JVF) at depth, and the first seconds of rupture involved deep slip. Rupture then continued shallowly on the JVF for the subsequent 4 sec. The region immediately local to the Landers epicenter, along the previously recognized and active Johnson Valley fault, saw many $M > 4$ aftershocks within the first 24 hours of the mainshock (Hauksson *et al.*, 1993). However, we were not able to obtain TERRAscope data for these early events. We examined two later events, one nearly colocated with the mainshock (Fig. 12, event 10) and one slightly northeast of the same, an M 4.7 event that occurred in June 1994 (Fig. 12, event 19). Both events are oblique slip, of moderate to shallow source depth, and are low stress drop (9 and 15 bars,

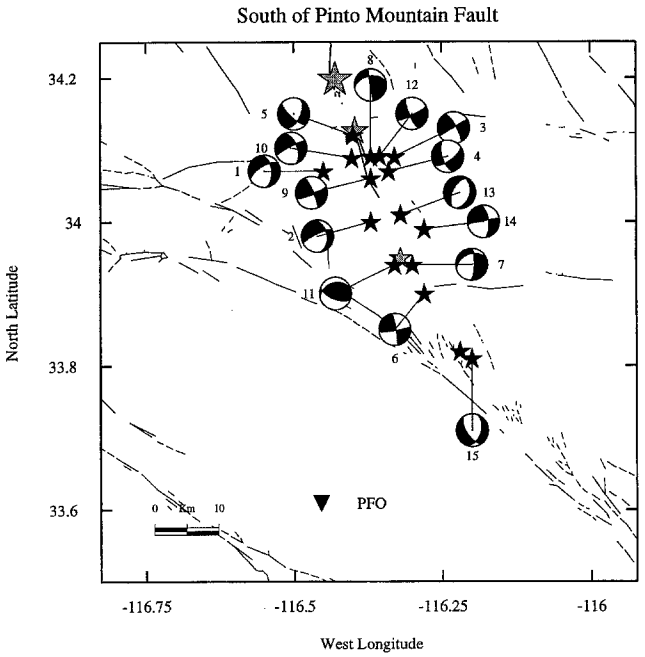

Figure 9. Map showing Landers aftershocks south of the Pinto Mountain fault. Locations of these aftershocks were previously shown relative to earlier Joshua Tree aftershocks (Fig. 7b). In this map, the aftershocks are numbered chronologically and listed in the same order in Table 4. The Joshua Tree mainshock is shown as a small filled (gray) star; Landers mainshock and southern Landers subevent are also shown as filled (gray) stars.

respectively, see Figs. 12 and 13), suggesting that stresses local to the mainshock epicentral area were fairly low in the months and hours following the Landers earthquake. Indeed, according to Abercrombie and Mori (1994), the mainshock itself began with a shallow, low stress-drop preshock composed of two $M \sim 4$ to 5 subevents (stress drops for both ~12 bars), which triggered or grew into the M 7.3 Landers mainshock.

Kickapoo (Landers) Fault. There were an unusual number of $M_w > 3.9$ aftershocks along the short segment of the newly recognized Kickapoo (Landers) fault. This is a previously unmapped, 5-km-long N–S-trending fault strand running from the northern leg of the Johnson Valley fault northward to the southernmost end of the Homestead Valley fault. Rupture during the 1992 Landers event propagated from the Johnson Valley fault to the Homestead Valley fault along the Kickapoo fault and secondary fault traces just east of the Kickapoo (Sowers *et al.*, 1994). We studied four (out of six) $M > 3.9$ aftershocks occurring along or near the Kickapoo fault that were recorded on the TERRAscope array (Fig. 12).

The earliest event is a normal-faulting event occurring near the southern end of the zone comprised of the Kickapoo and its secondary faults (Fig. 12, Table 5, event 1). It is of moderate stress drop (84 bars) and average depth for this region. It was followed by two strike-slip to oblique-slip events just north along the Kickapoo (Fig. 12, Table 5, events 3 and 9). The first of these is the largest aftershock to occur within the Landers rupture region, at $M_w = 5.2$, and also has the highest stress-drop (about 515 ± 176 bars). A second (M_w 3.9) colocated right-lateral strike-slip aftershock occurred two weeks later (event 9) at a depth of about 6 km. This event is substantially smaller, has a much lower stress drop (30 bars), and may represent rerupturing of a previously ruptured fault patch. A later M_w 4.3 event occurred near the southern end of the Homestead Valley fault approximately near the termination of the Kickapoo fault (Fig. 12, event 15). This aftershock is of similar depth (7 km), has an oblique-slip source mechanism, and a stress-drop of about 86 bars. It occurred within a region mapped and described by Spotila and Sieh (1995) and exhibited both strike-slip and thrust faulting. This region was associated with a slip gap during the Landers rupture and showed some vertical offset but virtually no strike-slip motion.

The presence of the latter three events lends support to the dominantly right-lateral offset throughgoing model suggested by Sowers *et al.* (1994) for the Kickapoo fault. However, the mechanism of the earliest large Kickapoo aftershock (event 1) suggests extension, which lends credence to the less favored "stepover model" suggested by Sowers *et al.* (1994). Clearly, the tectonics of the Kickapoo fault is more complicated than either of these simple schemes; perhaps some combination of the two models might explain the complex seismicity we observe here. The presence of so many heterogeneous and high stress-drop aftershocks along this small segment of fault also lends credence to the suggestion made by Spotila and Sieh (1995) that the connection between the Johnson Valley and Homestead Valley faults is incomplete and that the Kickapoo fault is still very immature.

Emerson and Camp Rock Faults. Large on-fault aftershocks appear to be much less common north of the Kickapoo Fault. Most $M > 3.9$ aftershock activity appears to be concentrated near the end of rupture on the Camp Rock fault. Relative stress drops on these faults are low to moderate, ranging from 38 to 86 bars for the events we studied (Table 4).

Off-Fault Aftershock Activity

In addition, there are clusters of large aftershocks off-fault (i.e., unrelated to any primary rupture during the Landers mainshock). These occurred east of the Landers rupture, near the Pisgah/Calico faults (Figs. 12 and 15) and north of the terminus of Landers rupture on the Camp Rock fault, in the Barstow region.

Aftershocks on Pisgah–Calico Faults. Aftershocks near the Calico fault (Fig. 11) form two east–west alignments perpendicular to the trend of the Landers rupture, roughly at the latitudes of the Emerson and Camp Rock faults (Fig. 6).

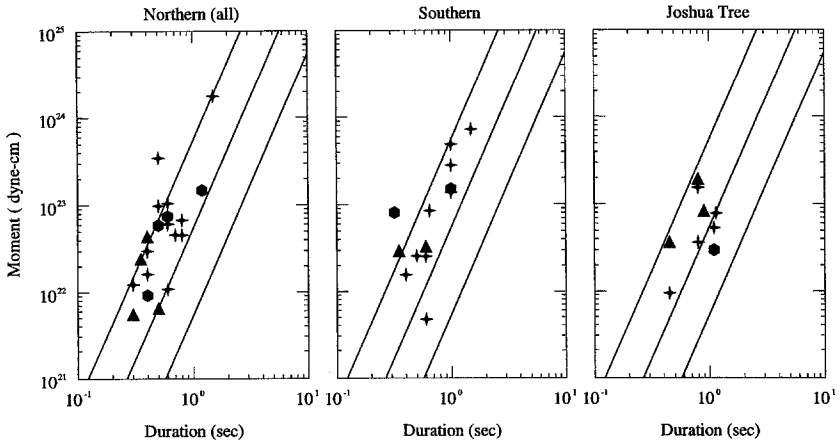

Figure 10. Moments versus durations for Joshua Tree aftershocks and Landers events both north and south of the Pinto Mountain fault. Event depths are indicated by different symbols: filled triangles indicate comparatively "deep" events (12 to 17 km); filled crosses indicate "intermediate" depth events (8 to 11 km); and filled hexagons indicate "shallow" events (2 to 7 km). Lines of constant stress drop are plotted diagonally across the figure; from bottom to top: 1, 10, and 100 bars. The first panel shows Landers events north of the Pinto Mountain fault, the second shows events south of the Pinto Mountain fault, and the third shows Joshua Tree events.

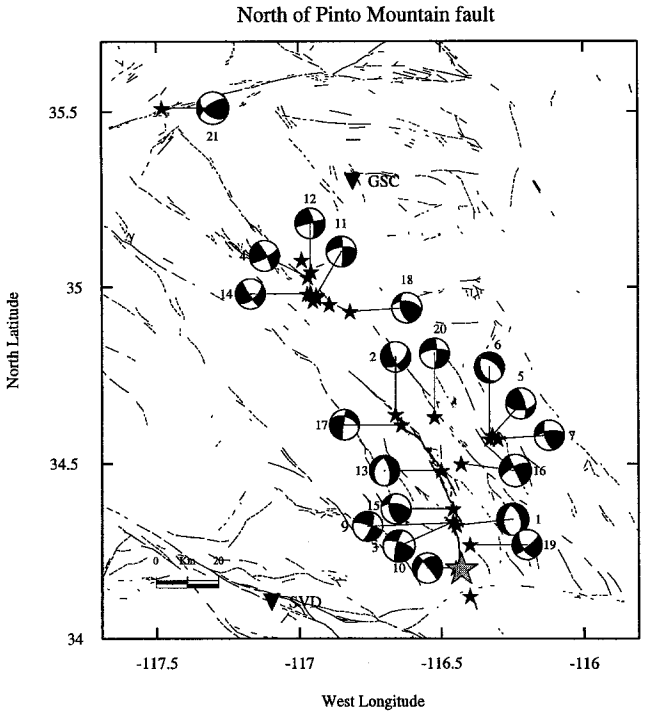

Figure 11. Map showing Landers aftershocks north of the Pinto Mountain fault, including off-fault clusters at Barstow, and on the Pisgah and Calico faults. Events are numbered in the order of occurrence and listed in this order in Table 5.

Stress drops for two $M > 4$ events (Fig. 11, events 16 and 20) are moderate to high; the latter event (20) occurred more than two years after the Landers mainshock but shows similar fault motion and depth as the earlier event (16) occurring in August 1992. In addition, there is a spatially and temporally tight cluster of aftershocks just east of the Pisgah fault, several of which are larger than M 4. Two of these occurred within an hour of each other and were nearly colocated (events 5 and 6), the second event having a lower relative stress drop (25 bars) than the first (71 bars). Aftershocks on the Pisgah and Calico faults may be related to off-fault strain caused by changes in strike along the Landers rupture (Sieh *et al.*, 1993). High stress drops in both regions might suggest high applied shear stresses along north to northwest-striking planes.

The Barstow Sequence. The Barstow cluster was associated with no surface rupture and occurred approximately 30 to 40 km north of the aftershocks associated with northernmost Landers rupture on the Camp Rock fault. It began approximately 6 h after the Landers mainshock and comprised at least 12 aftershocks above M 4. The largest aftershock, at $M_w = 4.4$, occurred on 5 August 1992, at 22:22 GMT, within a tight cluster of larger aftershocks toward the southern end of the trend (Fig. 13). The Barstow sequence is fairly narrow in width compared with aftershocks along the Landers rupture; the ratio of length (about 20 km) to width (2 to 3 km) has been cited as evidence that the Barstow sequence may have occurred on a single fault, unlike Landers (Hauksson *et al.*, 1993). However, closer examination of the larger aftershocks in the sequence shows a distinct jog in the trend of the aftershocks, with a tight cluster to the southeast (e.g., aftershocks 11 and 14 at depths of 8 and 7 km, respectively) that could arguably have occurred on a single fault. There is an abrupt stepover, with events farther to the west (events 4 and 11) along a rough trend striking NW–SE. Stress drops for these earthquakes range from 16 to 80 bars, with an average of about 50 bars. Our depth estimations do not show the shallowing reported by Hauksson *et al.* (1993), and shallowest events are at a depth of 5 km.

Aftershocks or Triggered Events on the Garlock Fault?

The Garlock fault has long been recognized as an important tectonic feature in southern California. Though it has not produced any large earthquakes within the period of historical record, numerous scarps and left-laterally offset Holocene features suggest that the fault is active and has produced large earthquakes. As recent levels of seismic activity on this fault are low in comparison to those inferred from Holocene displacements, the Garlock fault may represent a

Table 5
Landers Events, North of Pinto Mountain Fault

No.	Date	M_w	τ, $\Delta\sigma$ (s, bars)	θ	δ	λ	Location		
							Depth (km)	Latitude (°N)	Longitude (°W)
1.	92063012	4.0	0.30, 84	342	50	254	9	34.32	116.45
2.	92063017	4.1	0.40, 46	156	74	222	8	34.64	116.66
3.	92070107	5.2	0.50, 515	194	76	160	7	34.33	116.46
4.	92070510	4.5	0.80, 25	331	80	169	8	35.03	116.97
5.	92070521	5.4	1.50, 71	344	70	142	8	34.58	116.32
6.	92070522	4.4	0.70, 25	336	64	140	8	34.57	116.33
7.	92070802	4.6	0.50, 140	162	66	156	8	34.57	116.30
8.	92071118	5.3	0.55, 1044	296	58	164	11	35.21	118.07
9.	92071500	3.9	0.40, 30	20	68	186	6	34.33	116.46
10.	920720040	3.9	0.60, 9	320	84	224	8	34.20	116.45
11.	920720044	4.4	0.80, 16	358	82	204	7	34.96	116.95
12.	92072013	4.5	0.60, 63	348	71	183	5	34.98	116.96
13.	92072407	3.8	0.30, 38	344	60	260	11	34.48	116.50
14.	92080522	4.6	0.60, 80	146	82	210	6	34.98	116.97
15.	92080815	4.3	0.40, 86	168	64	146	8	34.37	116.45
16.	92083109	4.2	0.35, 78	154	90	160	12	34.50	116.43
17.	92100207	4.6	0.35, 250	189	83	313	5	34.61	116.64
18.	92101112	4.4	0.60, 52	170	64	140	8	34.93	116.82
19.	94061616	4.7	1.2, 13	148	61	193	5	34.267	116.40
20.	94080121	4.4	0.40, 126	360	78	202	14	34.633	116.523
21.	94101900	4.2	0.22, 190	126	50	150	8	35.51	117.48

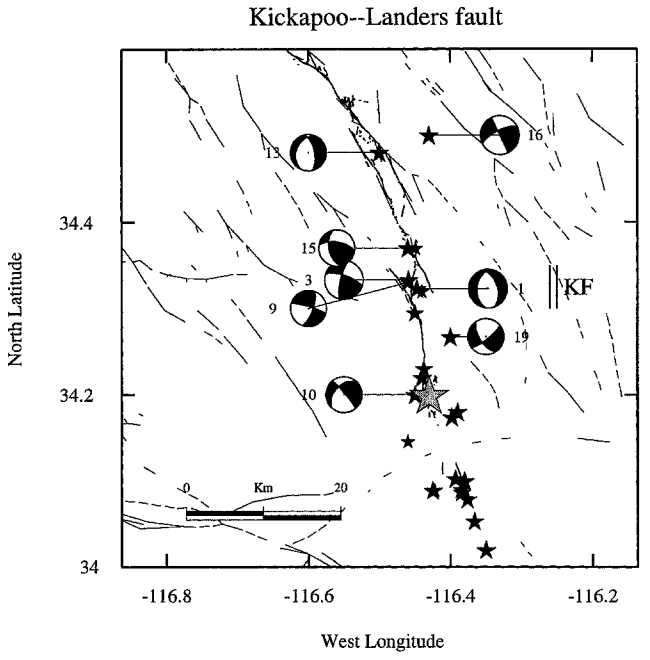

Figure 12. Detail of map from Figure 11, showing seismicity around the mainshock area (large gray star) and Kickapoo fault (indicated by double line and the letters KF). All events of $M > 4.0$ are shown. Most seismicity south of the Pinto Mountain fault and around mainshock epicenter occurred within the first 24 hours.

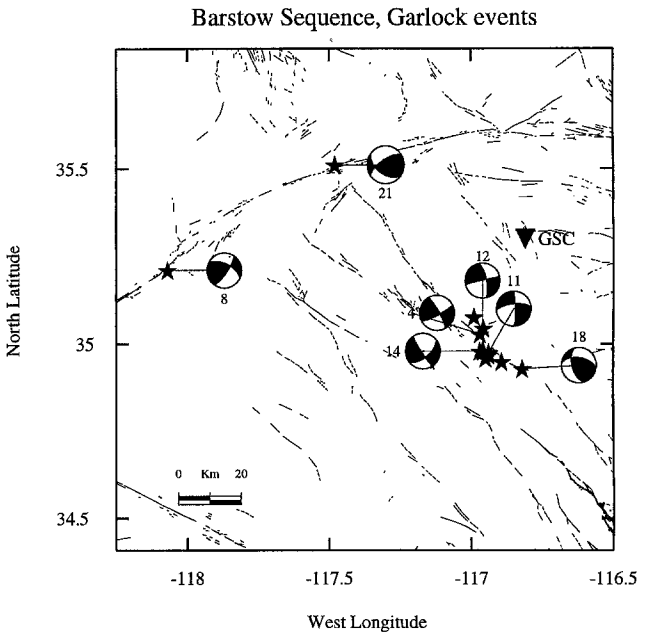

Figure 13. Detail of map from Figure 11, showing off-fault seismic activity in the Barstow area and farther north along the Garlock fault. Events are numbered as in Figure 11 and in Table 5.

seismic gap (Astiz and Allen, 1983). Until the moderately sized earthquakes in July 1992 (Fig. 13, event 8) and again in October 1994, (Fig. 13, event 21) no such earthquakes were known to have occurred on the Garlock fault, though there were several historical events for which a Garlock fault source was possible (McGill and Sieh, 1991).

The July 1992 event was the larger of the two recent events, at $M_w = 5.3$. This was the largest earthquake associated with the Garlock fault since the 10 June 1988, $M_L = 5.4$ earthquake that occurred several kilometers north of the Garlock, about 20 km east of its intersection with the San Andreas fault (McGill and Sieh, 1991). Prior to the 1988 event, the most recent earthquakes local to the Garlock fault were two historical events occurring in 1916: an M 5.5 event 45 km north of the eastern end of fault, in the Quail mountains (Toppozada *et al.,* 1978), and an M 5.2 earthquake at the western end of the fault, for which the San Andreas may be responsible. The 11 July 1992, M_w 5.3 Garlock earthquake was clearly related to and possibly triggered by the sudden changes in the regional stress field caused by Landers. The 1992 event and the 19 October 1994, M_w 4.0 earthquake lie on either side of the mid-point of the Garlock (near the city of Rand), which marks a change in strike, seismic and aseismic behavior, and geology (Astiz and Allen, 1983). The two events lie on either side of an en-echelon fault stepover near Rand and Koehn lake, which McGill and Sieh (1991) argue divides the fault into a western and an eastern segment.

While the western segment of the Garlock Fault has manifested continuous low-level seismicity and demonstrable creep during the last several decades, the eastern segment has had only a few small earthquakes and no observed creep (Astiz and Allen, 1983). The M_w 5.3 1992 event, which took place within two weeks of the Landers mainshock, occurred on the western segment very near the en-echelon stepover, at a depth of 11 km (Fig. 13, Table 5, event 8). This event was moderate in size, with a moment of $M_0 = (9.44 \pm 2.29) \times 10^{23}$ (from our long-period solution), but extremely short in source duration, which yields an unusually high stress drop of about 1044 $\pm$ 253 bars. Broadband and long-period waveform fits for the 11 July 1992 Garlock event are shown on Figures 14a and 14b, respectively. The broadband modeling yields a lower moment estimation, thus a slightly lower stress drop of 840 $\pm$ 316 bars. Error associated with moment determination is greater for the broadband records, which translates into higher error in the stress-drop estimation.

The M_w 4.0 1994 event occurred on the eastern segment of the Garlock, also near the en-echelon stepover, and had a stronger thrust component to its motion (Fig. 13, event 21) and a depth of about 8 km. The stress drop is lower than that obtained for the earlier event but nonetheless high: 192 $\pm$ 90 bars for the long-period solution. The presence of these arguably triggered, rare, high-stress-drop events on a seismically quiescent fault suggests that small patches of the fault may rupture energetically, in the first case at fairly great depth within the crust. This further suggests that the Garlock may be storing strain, especially near the stepover that marks a transition from creeping to locked behavior.

Summary

Because duration and moment are routinely computed for each event we study, we infer stress drops for these events, assuming a circular fault. Stress drops appear to vary systematically with location, with respect to previous seismicity or rupture, and in the case of events in the Transverse ranges only, with respect to depth (Fig. 15). Our event sample size is small in number for any given region, yet the events studied here are of moderate size (on average $M \sim 4.2$), thus associated with more energy release than smaller (and more numerous) events.

We have observed the following for events within the ECSZ:

- Joshua Tree events occurred in a historically active region, and though the sequence was relatively sustained given the mainshock size, average stress drops are low (30 bars) compared to aftershocks from the Landers sequence both north and south of the Pinto Mountain fault (Fig. 10).
- Almost 76% of total aftershock energy post-Landers was released south of the mainshock epicenter in the southern Landers area, yet stress drops for these events are about 50% lower, on average, than stress drops for events north of the Pinto Mountain fault (i.e., 67 bars for southern Landers, and 95 bars for on-fault and off-fault activity north of the Pinto Mountain fault, omitting Garlock events; see Fig. 10).
- Regions active during the Joshua Tree sequence form a stress drop low during the southern Landers sequence, and $M > 4$ events there were not numerous. This suggests that while the Landers mainshock may have recharged aftershock activity in the Joshua Tree region (Hauksson, 1994), moment release and stress drop in the region remained low.
- Heterogeneous and high stress-drop aftershocks occurred along the newly recognized Landers–Kickapoo fault, associated with smaller surficial slip on the Landers fault relative to the Johnson Valley fault (JVF) and the Homestead valley fault (HVF) and lack of throughgoing dextral rupture across the JVF/HVF stepover. High stress-drop events in this area may be related to the presence of the immature Landers fault and an incomplete connection between the Johnson Valley and Homstead Valley fault systems.
- High stress drops in the Pisgah–Calico region might suggest high applied shear stresses on north–south planes, while relative stress drops in historically active Barstow were appreciably lower, much like aftershocks in the Joshua Tree region.
- In the immediate aftermath of the Landers event, a large, rare, high-stress-drop event occurred on the historically quiescent Garlock fault. Two years later, a second event occurred near the stepover from the creeping western seg-

(a)

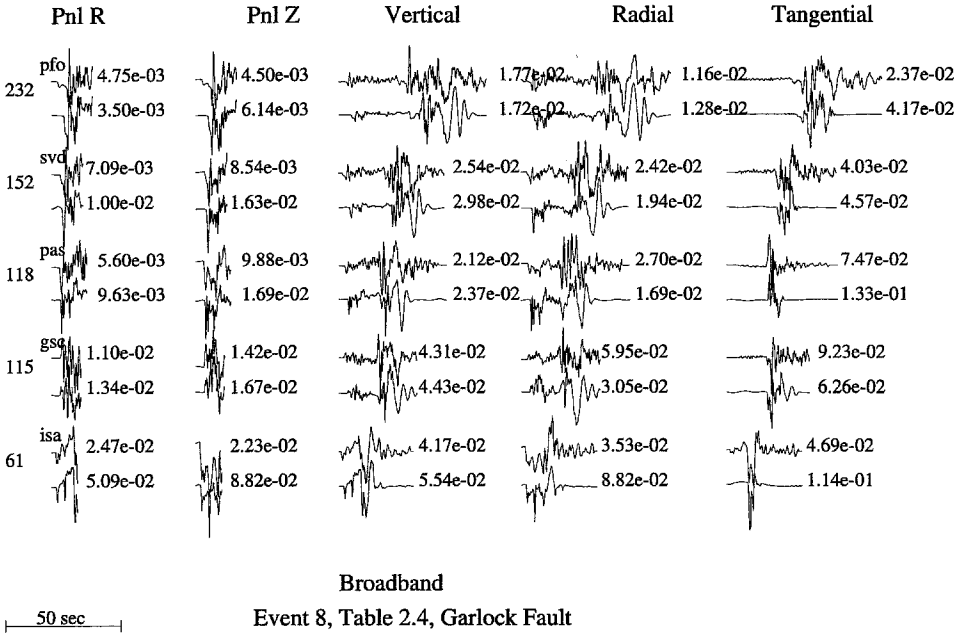

(b)

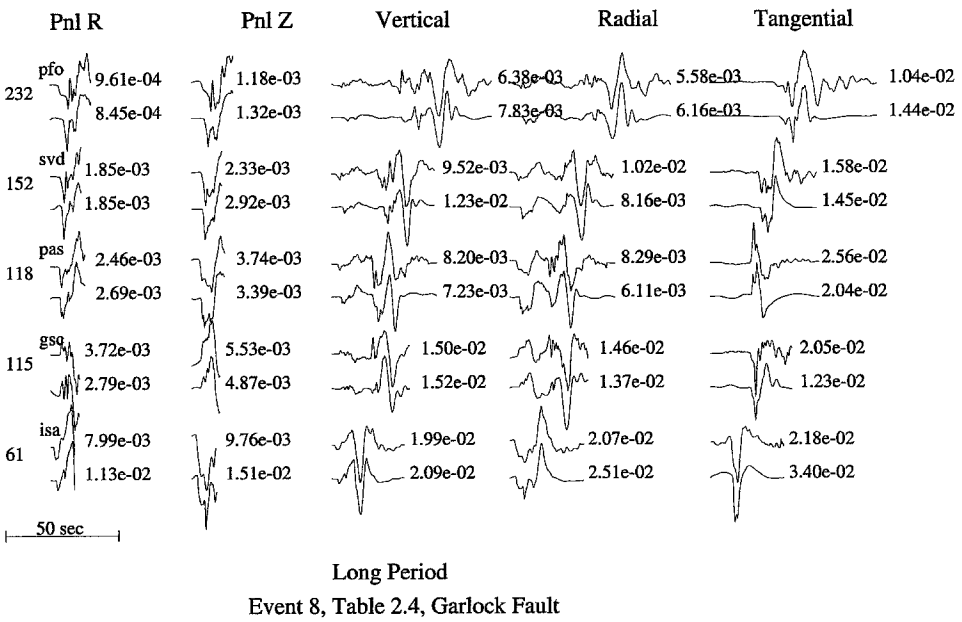

Figure 14. (a) Broadband waveform modeling for the M 5.3, 11 July 1992, Garlock earthquake. Both the standard southern California model (stations PAS and PFO) and Mojave model (GSC, ISA, and SVD) were used in this source estimation. The moment for this solution is $M_b = (7.64 \pm 2.85) \times 10^{23}$; the time function is (0.25, 0, 0.25) sec. (b) Long-period waveform modeling for the 11 July 1992, Garlock earthquake. Moment is $M_o = (9.44 \pm 2.29) \times 10^{23}$ for the long-period solution.

ment to the locked eastern strand of the fault. The presence of these two events on a historically aseismic fault suggests that small patches of a quiescent fault may rupture very energetically and also that the Garlock may be storing strain, especially at the stepover that marks a transition from creeping to locked behavior.

- In contrast to aftershocks from the Big Bear sequence, Landers aftershocks are in general shallower (Jones and Helmberger, 1996). Although Landers and Big Bear events are all moderately high stress drop (on average, 70 bars for the Landers events, 100 bars for Big Bear, see Fig. 15), events occurring in the eastern Transverse ranges are generally higher stress drop and show a strong correlation between high stress drop and greater event depth. Like

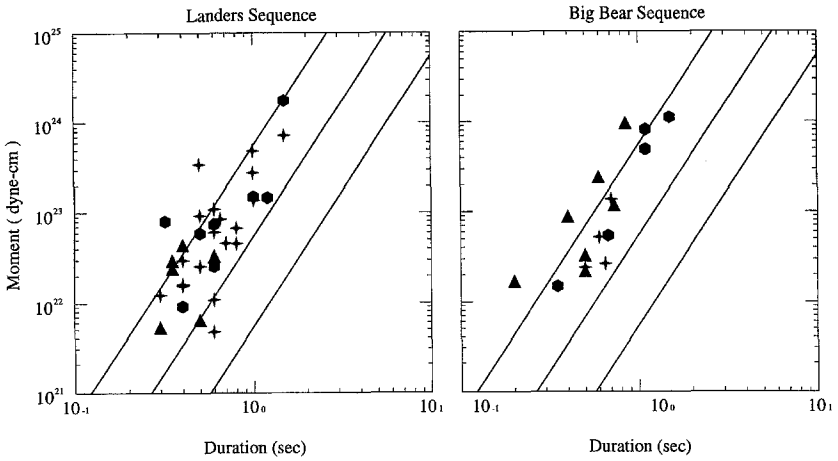

Figure 15. Moments versus durations for Big Bear and Landers aftershocks. Event depths are indicated as follows: filled triangles indicate deep events (12 to 17 km); filled crosses are intermediate (8 to 11 km), and filled hexagons are shallow (2 to 7 km). Lines of constant stress drop are plotted diagonally: from bottom to top, 1, 10, and 100 bars. Figure after Jones and Helmberger (1996).

events in the Transverse ranges, however, high stress drops for Landers events appear to correlate with activity on immature or low-slip faults.

Conclusions

The Landers mainshock and related events altered the tectonic landscape and stress budget of southern California in ways not yet fully assessed. The Landers earthquake itself involved surface rupture and displacement on six separate faults, including rupture south of the Pinto Mountain fault on the Eureka Peak fault. Aftershocks and triggered events occurred as far away as Mammoth Lakes, California, and Little Skull Mountain, Nevada (Hill *et al.*, 1993), and included the complex M 6.5 Big Bear mainshock and several unusual earthquakes on the Garlock fault.

For the Landers sequence, stress drops of events located at some distance from the Landers rupture are higher than those located on the faults involved in the mainshock, with the exception of aftershocks on the juvenile Kickapoo (Landers) fault. Rupture on this fault segment was complicated, and displacement may have been accommodated across a number of subsidiary or discontinuous fault traces. The fact that the Kickapoo fault had some of the lowest measured surface displacements during the Landers mainshock lends credence to this idea.

Aftershock stress-drop patterns often show a low associated with the mainshock fault plane. We observe an analogous phenomenon in the low stress drops recorded for previously active regions of the strike-slip system comprising southern and northern Landers. Work by Smith and Priestly (1993) on the 1984 Round Valley, California, earthquake showed an aftershock stress-drop minimum on the fault plane, suggesting nearly complete stress release in the ruptured area. Consistent with their work and with theories of fault rupture and asperity (Madariaga, 1973) is our observation that stress drops are relatively higher off-fault and around the edges of the rupture trace.

High stress drops have been associated with long earthquake recurrence times (Kanamori and Allen, 1986, which may in turn be related to low slip rates on locked, discontinuous, or youthful faults. In the aftermath of the Landers earthquake, an unusual, deep, high-stress-drop event was triggered on the Garlock fault, which has not experienced any large earthquakes within the period of historical record, though scarps and offset features suggest it has produced large earthquakes in the past. Here again is an example of a quiescent fault producing high-stress-drop events.

Aftershocks south of the Pinto Mountain fault occurred in a region associated with high rates of post-seismic deformation, like those in the Barstow region (Shen *et al.*, 1994). Lower-stress-drop aftershocks seem to occur in regions that previously experienced the most local moment release, that is, near the Eureka Peak fault and near the Joshua Tree mainshock epicenter.

Acknowledgments

We thank Rachel Abercrombie and an anonymous reviewer for helpful comments and suggestions. Contribution Number 5800, Division of Geological and Planetary Sciences, California Institute of Technology, Pasadena, California 91125. Los Alamos National Laboratory Report Number LA-UR-98-2813.

References

Abercrombie, R. and J. Mori (1994). Local observations of the onset of a large earthquake: 28 June 1992 Landers, California, *Bull. Seism. Soc. Am.* **84,** 725–734.

Astiz, L. and C. R. Allen (1983). Seismicity of the Garlock fault, California, *Bull. Seism. Soc. Am.* **73,** 1721–1734.

Brune, J. N. (1970). Tectonic stress and the spectra of seismic shear waves from earthquakes, *J. Geophys. Res.* **75,** 4997–5009.

Cohn, S. N., T. L. Hong, and D. V. Helmberger (1982). The Oroville earthquakes: a study of source characteristics and site effects, *J. Geophys. Res.* **87,** 4585–4594.

Dreger, D. S. and D. V. Helmberger (1991). Source parameters of the Sierra Madre earthquake from regional and local body waves, *Geophys. Res. Lett.* **18,** 2015–2018.

Eshelby, J. D. (1957). The determination of the elastic field of an ellipsoidal inclusion and related problems, *Proc. R. Soc. London Series A* **241,** 376–396.

Gomberg, J. and P. Bodin (1994). Triggering of the M_s = 5.4 Little Skull

Mountain, Nevada, earthquake with dynamic strains, *Bull. Seism. Soc. Am.* **84,** 844–853.

Hadley, D. and H. Kanamori (1977). Seismic structure of the Transverse Ranges, California, *Geol. Soc. Am. Bull.* **88,** 1469–1478.

Hardebeck, J. and E. Hauksson (1997). Patterns of stress drop in the 1994 Northridge aftershock sequence, *Bull. Seism. Soc. Am.* **87,** 1495–1501.

Hauksson, E. (1994). State of stress from focal mechanisms before and after the 1992 Landers earthquake sequence, *Bull. Seism. Soc. Am.* **84,** 917–934.

Hauksson, E., L. M. Jones, K. Hutton, and D. Eberhart-Phillips (1993). The 1992 Landers earthquake sequence: seismological observations, *J. Geophys. Res.* **98,** 19835–19858.

Helmberger, D. V. and G. R. Engen (1980). Modeling the long-period body waves from shallow earthquakes at regional ranges, *Bull. Seism. Soc. Am.* **70,** 1699–1714.

Hill, D. P. *et al.* (1993). Seismicity in the eastern United States remotely triggered by the *M*7.4 Landers, California earthquake of June 28, 1992, *Science* **260,** 1617–1623.

Hough, S. E. and D. S. Dreger (1995). Source parameters of the 4/23/92 *M*6.1 Joshua Tree earthquake and its aftershocks: empirical Green's function analysis of GEOS and TERRAscope data, *Bull. Seism. Soc. Am.* **85,** 1576–1590.

Hough, S. E., J. Mori, E. Sembera, G. Glassmoyer, C. Mueller, and S. Lydeen (1993). Southern surface rupture associated with the 1992 M7.4 Landers earthquake: Did it all happen during the mainshock? *Geophys. Res. Lett.* **20,** 2615–2618.

Jones, L. E. and D. V. Helmberger (1992). Broadband modeling of aftershocks from the Landers, Big Bear and Joshua Tree events, *EOS* **43,** 383.

Jones, L. E. and D. V. Helmberger (1996). Seismicity and stress drop in the eastern Transverse Ranges, southern California, *Geophys. Res. Lett.* **23,** 233–236.

Jones, L. E., D. V. Helmberger, and S. E. Hough (1993). Rupture process of the June 28, 1992, Big Bear earthquake, *Geophys. Res. Lett.* **20,** 1907–1910.

Jones, L. E. and S. E. Hough (1995). Analysis of broadband records from the 28 June, 1992, Big Bear, earthquake: evidence of a multiple-event source, *Bull. Seism. Soc. Am.* **85,** 688–704.

Kanamori, H. and C. R. Allen (1986). Earthquake repeat time and average stress drop, in *Earthquake Source Mechanics,* S. Das and C. H. Scholz (Editors), American Geophysical Union, Washington, D.C., 227–235.

Kanamori, H., H.-K. Thio, D. Dreger, E. Hauksson, and T. Heaton (1992). Initial investigation of the Landers, California, earthquake of June 28, 1992 using TERRAscope, *Geophys. Res. Lett.* **19,** 2267–2270.

King, G. C. P., R. S. Stein, and J. Lin (1994). Static stress changes and the triggering of earthquakes, *Bull. Seism. Soc. Am.* **84,** 935–953.

Lindley, G. T. and R. Archuleta (1992). Earthquake source parameters and the frequency of attenuation at Coalinga, Mammoth Lakes and the Santa Cruz Mountains, California, *J. Geophys. Res.* **97,** B10, 14137–14154.

Ma, Kuo-Fong (1993). Broadband waveform observations of local earthquakes, *Ph.D. Thesis,* California Institute of Technology, Pasadena.

Madariaga, R. (1973). Dynamics of an expanding crack, *Bull. Seism. Soc. Am.* **66,** 639–666.

McGill, S. F. and K. Sieh (1991). Surficial offsets on the Central and Eastern Garlock fault associated with prehistoric earthquakes, *J. Geophys. Res.* **96,** 21597–21621.

Mori, J. (1996). Rupture directivity and slip distribution of the M4.3 foreshock to the 1992 Joshua Tree earthquake, *Bull. Seism. Soc. Am.* **86,** 805–810.

Shen, Z.-K., D. D. Jackson, Y.-J. Feng, M. Cline, and M. Kim (1994). Postseismic deformation following the Landers earthquake, California, June 28, 1992, *Bull. Seism. Soc. Am.* **84,** 780–791.

Sieh, K. *et al.* (1993). Near-field investigations of the Landers earthquake sequence, April to July, 1992, *Science* **260,** 171–176.

Smith, K. D. and K. F. Priestly (1993). Aftershock stress release along active fault planes of the 1984 Round Valley, California, earthquake sequence applying a time-domain stress-drop method, *Bull. Seism. Soc. Am.* **83,** 144–159.

Song, X. J. and D. V. Helmberger (1997). Northridge aftershocks, a source study with TERRAscope data, *Bull. Seism. Soc. Am.* **87,** 1024–1034.

Sowers, J. M., J. R. Unruh, W. R. Lettis, and T. D. Rubin (1994). Relationship of the Kickapoo fault to the Johnson Valley and Homestead Valley faults, San Bernardino County, California, *Bull. Seism. Soc. Am.* **84,** 528–536.

Spotila, J. A. and K. Sieh (1995). Geologic investigations of a "slip gap" in the surficial ruptures of the 1992 Landers earthquake, southern California, *J. Geophys. Res.* **100,** 543–559.

Stein, R. S., G. C. P. King, and J. Lin (1992). Change in failure stress on the Southern San Andreas fault system caused by the 1992 Magnitude = 7.4 Landers earthquake, *Science* **258,** 1328–1332.

Thio, H. K. (1996). 1- Using short-period surface waves to study seismic source and structure. 2: Source complexity of large, strike-slip earthquakes, *Ph. D. Thesis,* California Institute of Technology, Pasadena.

Toppozada, T., D. L. Parke, and C. T. Higgins (1978). Seismicity of California, 1900–1931, *Calif. Div. Mines Geol. Special Rept. 135.*

Wald, D. J., and T. H. Heaton (1994). Spatial and temporal distribution of slip for the 1992 Landers, California, earthquake, *Bull. Seism. Soc. Am.* **84,** 668–691.

Zhao, L.-S. and D. V. Helmberger (1994). Source estimation from broadband regional seismograms, *Bull. Seism. Soc. Am.* **84,** 91–104.

Zhao, L.-S. and D. V. Helmberger (1996). Regional moments, energy levels, and a new discriminant, *Pure Appl. Geophys.* **146,** 281–304.

Zhu, L. and D. V. Helmberger (1995). Advancement in source estimation techniques using broadband regional seismograms, *EOS* **76,** no 46, F424.

Los Alamos National Laboratory
EES-5, MS-F665
Los Alamos, New Mexico 87545
(L. E. J.)

Seismological Laboratory, 252-21
California Institute of Technology
Pasadena, California 91125
(D. V. H.)

Manuscript received 3 March 1997.